Cement and Concrete Research 39 (2009) 482–489

Contents lists available at ScienceDirect

Cement and Concrete Research

journal homepage: http://ees.elsevier.com/CEMCON/default.asp

# Solid solution between Al-ettringite and Fe-ettringite ($Ca_6[Al_{1-x}Fe_x(OH)_6]_2(SO_4)_3\cdot 26H_2O$)

Göril Möschner [a,*], Barbara Lothenbach [a], Frank Winnefeld [a], Andrea Ulrich [a], Renato Figi [a], Ruben Kretzschmar [b]

[a] Empa, Swiss Federal Institute for Material Testing and Research, Überlandstrasse 129, CH-8600 Dübendorf, Switzerland
[b] Institute of Biogeochemistry and Pollutant Dynamics, ETH Zurich, CHN, CH-8092 Zürich, Switzerland

ARTICLE INFO

*Article history:*
Received 28 July 2007
Accepted 3 March 2009

*Keywords:*
Ettringite
Thermodynamic calculations
Hydration products

ABSTRACT

The solid solution between Al- and Fe-ettringite $Ca_6[Al_{1-x}Fe_x(OH)_6]_2(SO_4)_3\cdot 26H_2O$ was investigated. Ettringite phases were synthesized at different Al/(Al + Fe)-ratios ($=X_{Al,total}$), so that $X_{Al}$ increased from 0.0 to 1.0 in 0.1 unit steps. After 8 months of equilibration, the solid phases were analyzed by X-ray diffraction (XRD) and thermogravimetric analysis (TGA), while the aqueous solutions were analyzed by inductively coupled plasma optical emission spectroscopy (ICP-OES) and inductively coupled plasma mass spectrometry (ICP-MS). XRD analyses of the solid phases indicated the existence of a miscibility gap between $X_{Al,total} = 0.3$–0.6. Some of the XRD reflections showed two overlapping peaks at these molar ratios. The composition of the aqueous solutions, however, would have been in agreement with both, the existence of a miscibility gap or a continuous solid solution between Al- and Fe-ettringite, based on thermodynamic modeling, simulating the experimental conditions.



## 1. Introduction

Ettringite occurs in natural alkaline environments (like Ca-rich igneous rocks, contact metamorphosed Ca-rich sediments or bioclastic sediments cemented by gypsum) with different chemical compositions, e.g. $Ca_6(Al)_2(SO_4)_3(OH)_{12}\cdot 25H_2O$ [1], $Ca_6(Si,Al,B)_3(SO_4)_2(O,OH)_{12}(OH)_4\cdot 26H_2O$ [2] and $Ca_6(Al,Si)_2(SO_4)_2(B(OH)_4)(OH)_{12}\cdot 26H_2O$ [3]. Iron containing analogues $Ca_6(Fe(III)_{1.5}Al_{0.3}Mn(II)_{0.2})_2(SO_4)_{2.3}(B(OH)_4)_{1.2}(OH)_{12}\cdot 25H_2O$ [4] and $Ca_6(Si,Al,Fe)_2(SO_4)_3(Cl,OH)_x\cdot xH_2O$ [5] have been reported. The structure of these minerals has been well investigated (e.g. [6–10]). Ettringite and it analogues form hexagonal, prismatic crystals. In pure aluminum containing ettringite columns of $[Al(OH)_6]^{3-}$ octahedra are linked together by calcium ions. The (OH) groups are shared between Al-octahedra and Ca-polyhedra and each of the latter contains four water molecules, which are located on the outer surface of the columns. Al(III) can be substituted by Fe(III) as well as by e.g. Cd(II) and Cr(III) [11–14]. The sulfate tetrahedra can be partially or entirely replaced by e.g. $SeO_4^{2-}$ and $CrO_4^{2-}$ [15–17].

Ettringite occurs not only in natural environments, but is also formed during hydration of Portland cement and super-sulfated blast furnace slag cements [18]. It forms from the cement clinker phases aluminate (idealized $Ca_3Al_2O_5$) and ferrate (idealized $Ca_2(Al_xFe_{1-x})_2O_5$), gypsum/anhydrite ($CaSO_4\cdot 2H_2O$/$CaSO_4$) and water. The Fe(III) present in ferrite can either partly replace Al(III) in ettringite or in other hydrates form during cement hydration such as monosulfate ($Ca_4[Al_{1-x}Fe_x(OH)_6]_2(SO_4)\cdot 6H_2O$) or hydrogarnet ($Ca_6[Al_{1-x}Fe_x(OH)_4]_2(OH)_4$), or it can precipitate as $Fe(OH)_3$, or as Ca–Al–Fe-gel [19–26]. The differentiation between iron free and iron containing phases in the hydrated cement samples is very difficult by the methods commonly used in cement chemistry (i.e. X-ray diffraction (XRD), thermogravimetric analysis (TGA), environmental scanning electron microscopy (ESEM), Raman spectroscopy), since the structural modification of the crystals is small and therefore difficult to detect. Pure iron containing ettringites ($Ca_6[Fe(OH)_6]_2(SO_4)_3\cdot 26H_2O$) have been synthesized and their solubility has been determined [12,27–29]. Buhlert and Kuzel [11] investigated the solid solution series between Al- and Fe-ettringite. They suggested a possible miscibility gap between 20 and 30 mol% Al ($X_{Al} = 0.2$–0.3), but the results were ambiguous, since the detected peak broadening was weak. Neubauer et al. [30] stated that ettringite phases immediately formed after the mixing of cement with water show a high substitution of aluminum by iron and of sulfate by carbonate. They performed in-situ X-ray diffraction and evaluated their data with Rietveld refinement. Neubauer et al. [30] found that the *c* lattice parameter of ettringite is highest at the very early hydration period of the cement. During the induction period they observed a decrease of the *c* parameter. From that they concluded that probably the ettringite crystals ripe, incorporating aluminum and sulfate.

The goal of this study was to examine the formation of solid solutions of the system $Ca_6[Al_{1-x}Fe_x(OH)_6]_2(SO_4)_3\cdot 26H_2O$ and to determine the solubilities of the solid phases. The different solids were

* Corresponding author. Empa, Laboratory for Concrete & Construction Chemistry, Ueberlandstrasse 129, CH-8600 Duebendorf, Switzerland. Tel.: +41 44 823 4788; fax: +41 44 823 4035.
*E-mail address:* gmoeschner@environcorp.com (G. Möschner).

0008-8846/$ – see front matter © 2009 Elsevier Ltd. All rights reserved.
doi:10.1016/j.cemconres.2009.03.001

synthesized and a thermodynamic model was established and compared to the experimental results of the solid and the liquid phases.

## 2. Methods

### 2.1. Synthesis of the solid solution series

A solid solution series $Ca_6[Al_{1-x}Fe_x(OH)_6]_2(SO_4)_3\cdot 26H_2O$ was synthesized by adding freshly prepared CaO, $Fe_2(SO_4)_3\cdot 5.3H_2O$ and/or $Al_2(SO_4)_3\cdot 16.2H_2O$ to 0.032 M KOH-solution. The amounts of the reactants were varied in that way that $X_{Al,total}$ increased from $X_{Al,total}=0.0$ to $X_{Al,total}=1.0$ in 0.1 unit steps; the liquid/solid ratio was constant ($l/s=10$) in all experiments. $X_{Al,total}$ is defined as the molar ratio of Al added to the system: $X_{Al,total}=\frac{x_{Al}}{x_{Al}+x_{Fe}}$, where $x_{Al}$ are the moles of Al and $x_{Fe}$ are the moles of Fe added to the system.

The mixtures were stored in sealed PE bottles and shaken at 20 °C for eight months. In contrast to Al-ettringite, where equilibrium is reached after a couple of days [31], for Fe-ettringite equilibrium is reached only after approximately 6 months [29]. Therefore the different mixtures of the solid solution series were equilibrated for 8 months.

After equilibration, the solid and the liquid phases were separated by vacuum filtration through 0.45 µm nylon filters. Both the mixing and the filtration were done in a $N_2$-filled glove box ($N_2$ was continuously bubbled through KOH-solution) to minimize $CO_2$ contamination. Afterwards the solid and the liquid phases were analyzed to characterize the precipitates and the dissolved concentrations of the different elements.

### 2.2. Characterization of the solid phases

After separating the liquid and solid phases, the solid precipitates were dried for three weeks in $N_2$-filled desiccators over saturated $CaCl_2$ solution; relative humidity was approximately 30%. The dry solid phases (masses of the solid phases amounted to 3.7 g–4.8 g for each sample) were ground by hand with an agate mortar in a $N_2$-filled glove box to <63 µm and analyzed by X-ray diffraction (XRD) and thermogravimetric analysis (TGA). For environmental scanning electron microscopy (ESEM) studies, a part of the dry solid phases was not ground but freshly fractured.

The XRD analyses were performed on a PANalytical X'Pert PRO system using $CuK_\alpha$ radiation (generator: 40 kV and 40 mA). The samples were transferred by backloading into specimen holders of 16 mm diameter. The measurement was carried out between 5 and 80° 2$\theta$ with a measuring speed of approximately 0.1°/s. For evaluation of the data the software X'Pert HighScore Plus V. 2.0a was used. To determine the lattice parameters of the different synthesized phases the following evaluation steps were carried out: first the background was set manually, and then a peak search was performed followed by a profile fitting. The indexing of the reflections was done using the Treor method. Approximately 45 reflections up to 75° 2$\theta$ were used for indexing. The cell parameters were then refined by least square algorithm. These cell parameters served as input for a Rietveld refinement of the lattice parameters using the ettringite structure published by Goetz-Neunhoeffer and Neubauer [38]. The refined parameters were background (5th order polynom), specimen displacement, scale factor, lattice parameter, profile parameters *U*, *V*, *W* (Pseudo Voigt profile), and preferred orientation in (100).

For TGA (Mettler Toledo TGA/SDTA851$^e$) about 8–12 mg of the ground sample was heated under $N_2$ over a temperature range of 30 to 980 °C at a rate of 20 °C/min.

The weight loss measured by TGA was used to calculate the amount of ettringite formed assuming that up to 300 °C only water evaporated ($Ca_6[Al_{1-x}Fe_x(OH)_6]_2(SO_4)_3\cdot 26H_2O$–$32H_2O \leftrightarrows 3CaO\cdot[Al_{1-x}Fe_xO_{1.5}]_2\cdot 3CaSO_4$).

ESEM studies were performed on Philips ESEM FEG XL 30 using low vacuum mode (at approximately 1 Torr $H_2O$).

### 2.3. Characterization of the liquid phase

One part of the liquid phases of each sample was instantly diluted (1:10 for inductively coupled plasma optical emission spectroscopy (ICP-OES) and 1:100 for inductively coupled plasma mass spectrometry (ICP-MS)) with nitric acid (diluted 1:10 from Merck $HNO_3$ suprapur quality, 65%, with high-purity water (18.2 MΩ/cm), prepared by a MilliQ-Gradient A10 System (Millipore)) in order to stabilize metals in solution and prevent the adsorption of the dissolved ions into the PE vials used. Another part of each sample was left untreated to measure the pH-value. This was done without any delay to minimize $CO_2$-contamination. Prior to the measurements the pH-meter (Knick pH-Meter 766 with a Knick SE 100 pH/Pt 1000 electrode) was calibrated with 0.001 to 1.0 M KOH-solutions.

The concentrations of calcium, sulfur and potassium were measured by ICP-OES (Varian, VISTA Pro) and the concentration of aluminum and iron by ICP-MS (Finnigan MAT, ELEMENT2).

### 2.4. Thermodynamic modeling

Thermodynamic modeling was carried out using the geochemical code GEMS [32]. GEMS is a broad-purpose geochemical modeling code, which computes equilibrium phase assemblage and speciation in a complex chemical system from its total bulk elemental composition. Chemical interactions involving solids, solid solutions, gas mixture and aqueous electrolyte are considered simultaneously. The default database of GEMS code was used, which is based on the PSI chemical thermodynamic database [33].

The Gibbs free energy of formation at 25 °C of the ettringite phases was adjusted to 20 °C using following equation:

$$\begin{aligned}\Delta_a G_T^0 &= \Delta_f G_{T_0}^0 - S_{T_0}^0(T-T_0) - \int_{T_0}^{T}\int_{T_0}^{T}\frac{C_p^0}{T}dTdT \\ &= \Delta_f G_{T_0}^0 - S_{T_0}^0(T-T_0) - a_0\left(T\ln\frac{T}{T_0} - T + T_0\right) \\ &\quad - 0.5a_1(T-T_0)^2 - a_2\frac{(T-T_0)^2}{2T\cdot T_0^2} - a_3\frac{2\left(\sqrt{T}-\sqrt{T_0}\right)^2}{\sqrt{T_0}}\end{aligned} \quad (1)$$

Where $\Delta_a G^0$ is the apparent Gibbs free energy of formation at any given temperature, which refers to the Gibbs free energy of the elements at 25 °C, $T$ = the given temperature (293.15 K in this study), $T_0=298.15$ K, $S^0$ is the entropy, $C_p^0$ is the heat capacity and $a_0$, $a_1$, $a_2$ and $a_3$ are empirical coefficients (see Eq. (2)).

$$C_p^0 = a_0 + a_1T + a_2T^{-2} + a_3T^{-0.5}. \quad (2)$$

A more detailed description of the temperature correction used in GEMS is given in [34–35].

Activity coefficients of aqueous species $\gamma_i$ were computed with the built-in expanded extended Debye–Hückel equation in Truesdell–Jones form with individual parameters $a_i$ and common third parameter $b_\gamma$ [33]:

$$log\gamma_i = \frac{-A_\gamma z_i^2\sqrt{I}}{1+B_\gamma a_i\sqrt{I}} + b_\gamma I \quad (3)$$

where $z_i$ denotes the charge of species $i$, $I$ the effective molal ionic strength, $b_\gamma=0.064$, and $A_\gamma$ and $B_\gamma$ are *P,T*-dependent coefficients. This activity correction is thought to be applicable up to 1–2 m ionic strength [32,36].

## 3. Experimental results

### 3.1. Solid phases of the solid solution series

X-ray diffraction patterns of the solid phases are presented in Fig. 1. For the solid solution series $Ca_6[Al_{1-x}Fe_x(OH)_6]_2(SO_4)_3 \cdot 26H_2O$ a shift of the reflections to lower *d*-values (i.e. to higher 2Θ values) was observed as $X_{Al,total}$ increased. This is due to the smaller ion radius of aluminum (0.51 Å) compared to iron (0.64 Å) [37]. For four reflections (2Θ ≈ 19, 23, 29, and 35° (*hkl* data: 104, 114, 116 and 216, cf. Table 1), dashed lines in Fig. 1a) two overlapping peaks between $X_{Al,total} = 0.3$ and $X_{Al,total} = 0.6$ were observed. The presence of two reflections indicates that in the Al- and Fe-ettringite solid solution series a miscibility gap exists. The absence of overlapping peaks for the main reflection at 2Θ ≈ 9°; $CuK_\alpha$ radiation (see Table 1) could indicate a continuous solid solution. However, the main reflections of pure Al- and Fe-ettringite are very close to each other (cf. Fig. 1b and Table 1). Thus, this reflection cannot be used for the interpretation of an existing miscibility gap and/or continuous solid solution.

**Table 1**
Selected reflections of X-ray diffraction powder patterns of Al- and Fe-ettringite.

| 2Θ Cu Kα | | | | |
|---|---|---|---|---|
| *hkl* | Al-ettringite [40] | Al-ettringite[a] this study | Fe-ettringite [28] | Fe-ettringite[a] this study |
| 100 | 9.091 | 9.130 | 9.131 | 9.115 |
| 104 | 18.911 | 18.912 | 18.539 | 18.525 |
| 114 | 22.944 | 22.937 | 22.662 | 22.634 |
| 116 | 29.645 | 29.631 | 29.099 | 29.075 |
| 216 | 35.023 | 34.985 | 34.598 | 34.566 |

[a] Samples contained 10% $SiO_2$ as internal standard and were displacement corrected.

The *c*-axis of pure Fe-ettringite equaled approximately 22.0 Å. With increasing amount of Al(III) incorporated in the solid phase the length of the *c*-axis decreased (Fig. 2a) to about 21.5 Å. This shift of 0.5 Å is again in accordance to the different ionic radii of aluminum and iron. In contrast, the determined length of the *a*-axis in the ettringite lattice increased when more Al(III) entered the solid phase (Fig. 2b). For pure Al-ettringite the determined value was about 11.24 Å, while for pure Fe-ettringite a value of about 11.19 Å was found. This shift of 0.05 Å of the *a*-axis was ten times smaller than the shift of

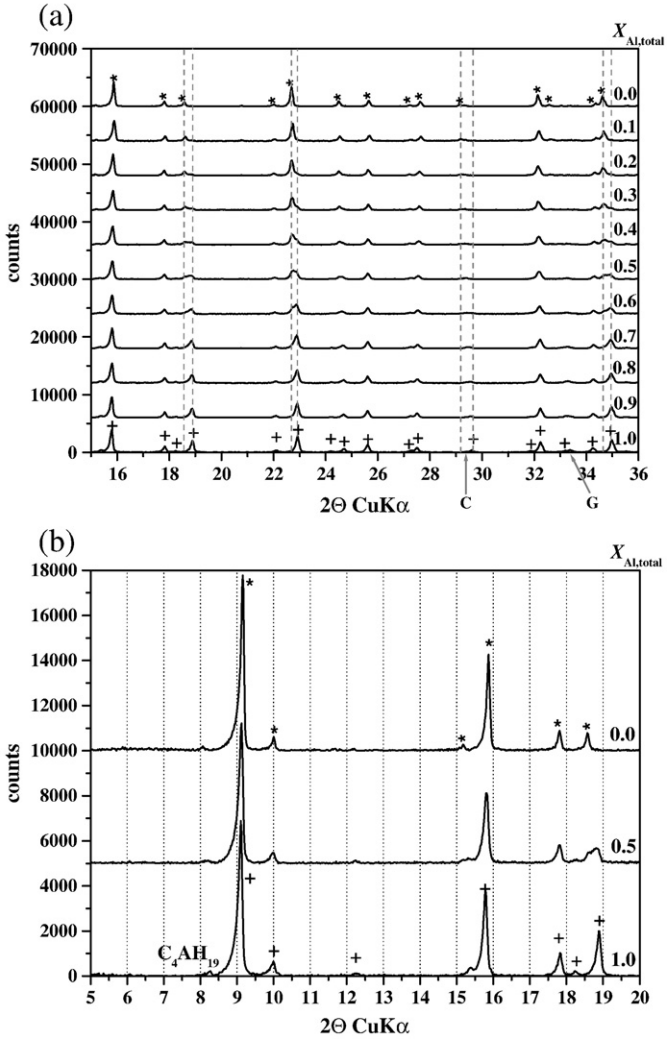


**Fig. 1.** X-ray diffraction spectra for ettringite synthesized with different $X_{Al,total}$ ratios. (a) *: Fe-ettringite (main peak at 2Θ = 9.13 [28]; +: Al-ettringite (main peak at 2Θ = 9.09); C: calcite (main peak at 2Θ = 29.62); G: gypsum (main peak at 2Θ = 11.59). The dashed lines mark the reflections with two overlapping peaks between $X_{Al,total}$ = 0.3 and $X_{Al,total}$ = 0.6. (b) *: Fe-ettringite (main peak at 2Θ = 9.13 [28]; +: Al-ettringite (main peak at 2Θ = 9.09), $C_4AH_{19}$: $Ca_4[Al(OH)_6]_2(OH)_2 \cdot 12H_2O$ (main peak at 2Θ = 8.30).

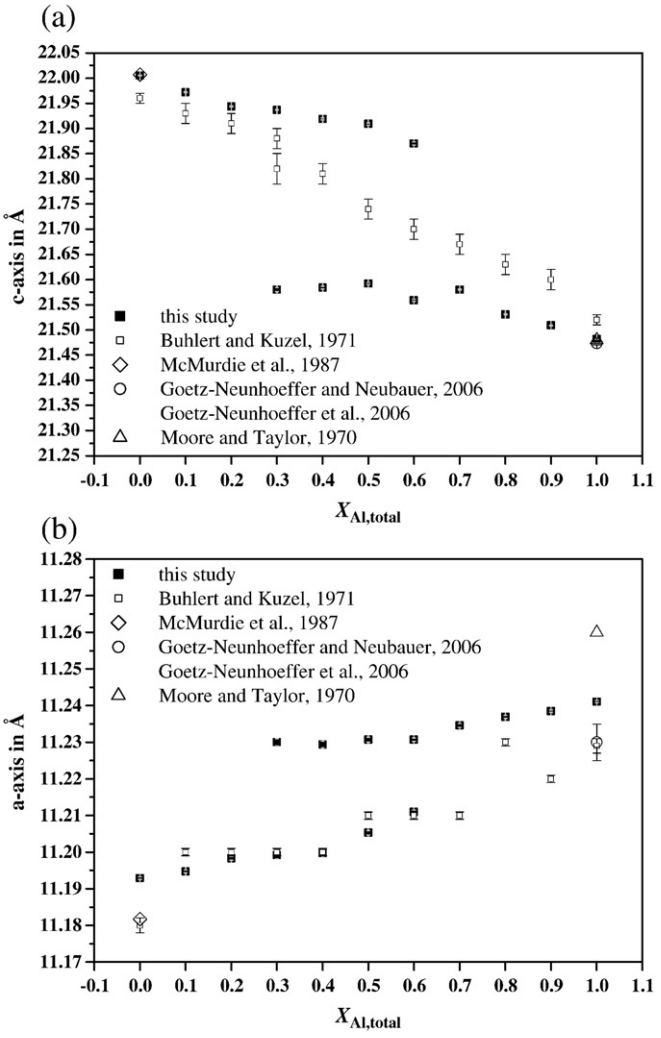


**Fig. 2.** Values of the *c*-axis (a) and the *a*-axis (b) determined by XRD for ettringite synthesized with different $X_{Al,total}$ ratios. Reference code: Buhlert and Kuzel: [11]; McMurdie et al.: [28]; Goetz-Neunhoeffer and Neubauer: [38]; Goetz-Neunhoeffer et al.: [39]; Moore and Taylor: [40].

the *c*-axis. This increase of the *a*-axis when more Al(III) entered the solid phase cannot be explained by the different ionic radii. It can only be stated that due to the decrease of the *c*-axis and the increase of the *a*-axis a compression occurs on the ettringite lattice when more aluminum enters the solid phase. For comparison Fig. 2 also shows the determined values of the *a*- and *c*-axis of previous studies [11,28,38–40]. Considering both, the observation of two overlapping peaks and the steep decrease (increase, respectively) of the lattice parameters between $X_{Al,total} = 0.3$ and 0.6, a miscibility gap between $X_{Al,total} = 0.3$ and 0.6 is possible (contrary to the study of Buhlert and Kuzel [11], who suggested a miscibility gap between $X_{Al,total} = 0.2$–0.3).

Furthermore traces of other phases were detected:

- from $X_{Al,total} = 0.5$ to 1.0, $C_4AH_{19}$, $Ca_4[Al(OH)_6]_2(OH)_2 \cdot 12H_2O$,
- from $X_{Al,total} = 0.6$ to 1.0, gypsum, $CaSO_4 \cdot 2H_2O$,
- and since TGA analysis revealed traces of $CO_2$, traces of calcite, $CaCO_3$ seemed to be in the system from $X_{Al,total} = 0.0$ to 1.0 (despite special attention to exclude $CO_2$ intrusion during sample preparation).

Thermogravimetric analysis showed that the ettringite phases lost their water molecules between 30 and 150 °C (cf. Fig. 3). Besides the loss of water the loss of traces of $CO_2$ between 625 and 700 °C, which is an evidence for calcite, was detected. In Fig. 3a the loss of weight during heating is presented for three selected samples: $X_{Al,total} = 1.0$, $X_{Al,total} = 0.5$ and $X_{Al,total} = 0.0$. The sample $X_{Al,total} = 1.0$ showed a slightly higher loss of weight than the sample $X_{Al,total} = 0.5$ and $X_{Al,total} = 0.0$. The more iron that is present in the solid phase the "heavier" is the solid phase and the smaller is the proportion of the water in the solid phase. The theoretical total weight loss of Al-ettringite is about 45.9% and of Fe-ettringite 43.9%. This difference of 2% is almost the same difference as measured in these experiments (43.7% and 41.6%, respectively). Al-ettringite loses its water mainly between 30 and 150 °C; a small additional maximum is visible in the derivative weight curve at approximately 250 °C (Fig. 3b). This is in accordance to findings of other studies [11,27,31] which assigned this additional maximum to Al-ettringite. However, for pure Fe-containing ettringite this peak and thus the loss of water at this temperature, was not observed [11,27].

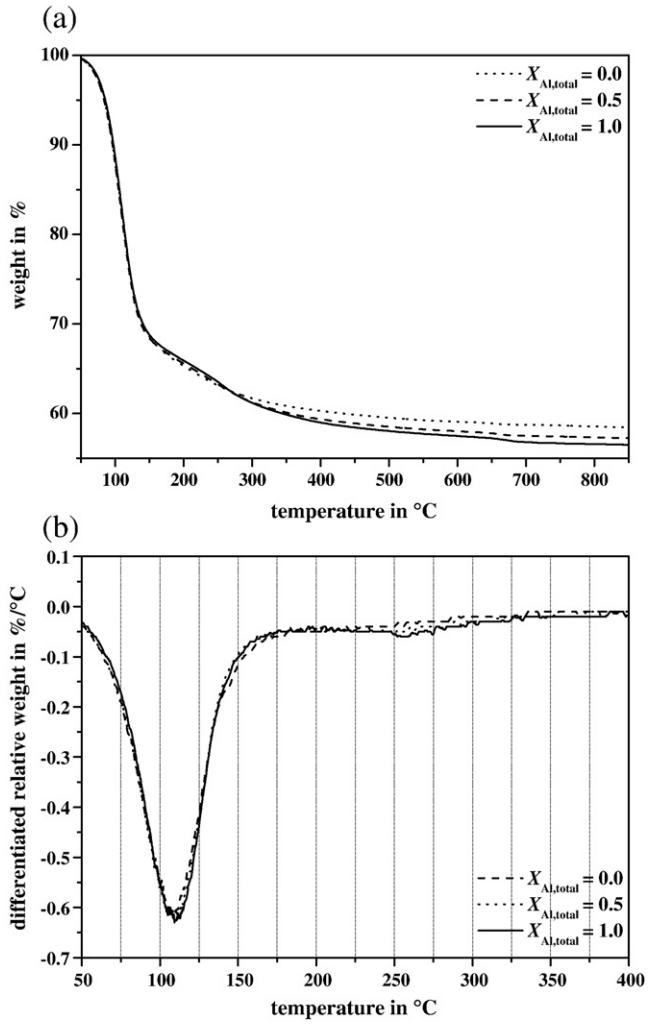


**Fig. 3.** (a) Weight loss of the solid phases at the $X_{Al,total}$ ratios of 0.0, 0.5 and 1.0 during TGA measurements. (b) Derivative curves of thermogravimetric analysis for ettringite synthesised at the $X_{Al,total}$ ratios of 0.0, 0.5 and 1.0.

**Table 2**
Weight of the solid phases after drying.

| $X_{Al,total}$ | Ettringite [g] | Calcite [g] | Sum of the solid phases [g] |
|---|---|---|---|
| 0.0 | 4.63 | 0.03 | 4.66 |
| 0.1 | 3.96 | 0.04 | 4.00 |
| 0.2 | 4.80 | 0.05 | 4.85 |
| 0.3 | 4.13 | 0.04 | 4.17 |
| 0.4 | 3.98 | 0.04 | 4.02 |
| 0.5 | 4.19 | 0.05 | 4.24 |
| 0.6 | 4.29 | 0.07 | 4.36 |
| 0.7 | 4.34 | 0.07 | 4.41 |
| 0.8 | 4.05 | 0.05 | 4.10 |
| 0.9 | 3.71 | 0.05 | 3.76 |
| 1.0 | 3.68 | 0.06 | 3.74 |

Masses of ettringite and calcite calculated from TGA measurements.

TGA analyses indicated for the ettringite phases in the presence of saturated $CaCl_2$ solutions a total water content of 30 to 31 $H_2O$ molecules. From the loss of water of the solid phases the masses of the different phases were calculated. The mass of calcite was calculated from the $CO_2$ weight loss. The results are presented in Table 2.

As discussed in Möschner et al. [29], the formation of Fe-hydroxide at low molar ratio of $X_{Al,total}$ is likely and was indicated by the slight reddish color of the these samples. But freshly precipitated Fe-hydroxide is XRD amorphous and thus difficult to detect. TGA reference curves of $Fe(OH)_3$, lepidocrocite and goethite (Fig. 4) showed that the loss of water of X-ray amorphous Fe-hydroxide overlapped with the loss of water of ettringite. Hence, the formation of Fe-hydroxides could not be excluded and the molar ratios of Fe and Al incorporated in the solid phases are not exactly known. Therefore, $X_{Al,total}$ is given always in this article which refers to the total amount of aluminum added to the system (see Section 2.1).

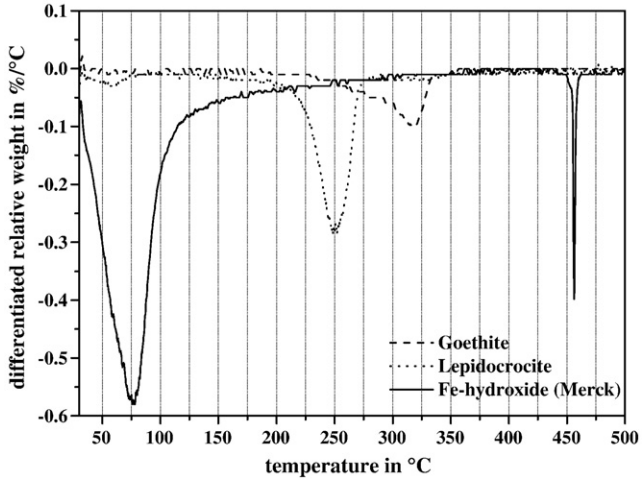


**Fig. 4.** Derivative curves of thermogravimetric analyses of $Fe(OH)_3$ (Merck), lepidocrocite, and goethite.

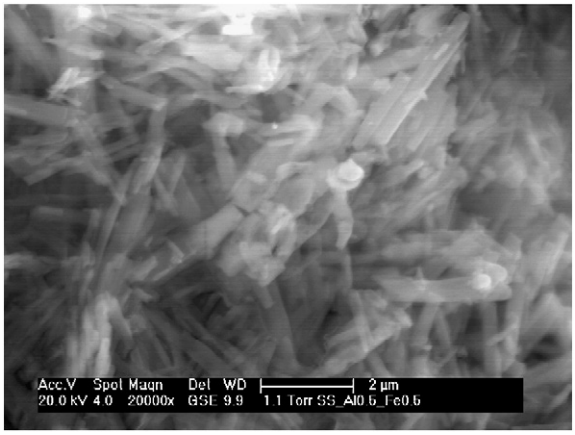


**Fig. 5.** Microstructure of ettringite at $X_{Al,total} = 0.5$ (ESEM).

ESEM studies showed that both, Al- and Fe-ettringite, precipitated in their typically needle-like shape. Fig. 5 shows one picture for $X_{Al,total} = 0.5$ as an example. The shape of the ettringite needles did not change significantly at different $X_{Al,total}$ ratios. ESEM studies also revealed the presence of some poorly or non-crystalline areas.

### 3.2. Liquid phase of the solid solution series

Analyses of the liquid phases of the solid solution series gave information about the composition of the aqueous solution in equilibrium with the different solid phases. The results are presented in Table 3.

The concentration of the dissolved iron in the aqueous solutions was in the range of 0.0 to 1. 3 µmol/L. The lowest concentration was obtained when iron is the dominating element in the solid phase ($X_{Al,total} = 0.0$ and 0.1). At higher ratios of $X_{Al,total}$ the iron concentration was slightly higher. Nevertheless, at a ratio of $X_{Al,total} = 1.0$, where no Fe-sulfate has been added, iron could be detected (Table 3).

The concentration of aluminum in the aqueous solutions of the different solid phases showed its maximum at the ratios of $X_{Al,total} = 1.0$ and $X_{Al,total} = 0.9$. Then it decreased rapidly and remained constant at about 10 µmol/L at lower $X_{Al,total}$ values. But it cannot be excluded that the measured low concentration of aluminum in the samples at ratios between $X_{Al,total} = 0.8$ and 0.0 was due to contamination, since in the used KOH-solution, which was treated like the samples, also an Al concentration about 10 µmol/L could be detected, even though special attention was paid to exclude contamination.

The highest calcium and sulfur concentrations occurred at a ratio of $X_{Al,total} = 0.0$, i.e. in the absence of aluminum. Both, calcium and sulfur, decreased between $X_{Al,total} = 0.0$ and $X_{Al,total} = 0.8$. At $X_{Al,total} = 0.9$ to 1.0 significant lower concentrations were measured. Thus the low iron concentrations, which are limited by the presence of Fe-hydroxide, were reflected in higher calcium and sulfur concentrations, while the relatively high aluminum concentrations led to lower Ca and S concentrations in the aqueous solutions.

## 4. Thermodynamic modeling

The ion concentrations and the solubility of $Ca_6[Al_{1-x}Fe_x(OH)_6]_2(SO_4)_3 \cdot 26H_2O$ ($x = 0.0, 0.1, 0.2, \ldots, 1.0$) at 20 °C were calculated using the geochemical code GEMS [32]. The thermodynamic data used are compiled in Table 4. Lothenbach et al. [41] give for Al-ettringite a solubility product of $\log K_{S0,\ Al\text{-ettringite}} = -44.9 \pm 0.7$ at 25 °C for the reaction

$$Ca_6[Al(OH)_6]_2(SO_4)_3 \cdot 26H_2O \leftrightarrows 6Ca^{2+} + 2Al(OH)_4^- + 3SO_4^{2-} + 4OH^- + 26H_2O. \quad (4)$$

Using the data given in Table 5 and using Eq. (1) this refers to a solubility product of $\log K_{S0,\ Al\text{-ettringite}} = -45.5 \pm 0.7$ at 20 °C. The thermodynamic data of the ion species used for calculating the Gibbs free energy of reaction at 20 °C as well as at 25 °C are presented in Table 6. For Fe-ettringite a solubility product of $\log K_{S0,\ Fe\text{-ettringite}} = -44.7 \pm 0.7$ has been measured at 20 °C [29]. For modeling the solid solution series between Fe- and Al-ettringite, the total solubility product was normalized so that the number of exchangeable sites was reduced to 1: $Ca_3[Al_{1-x}Fe_x(OH)_6](SO_4)_{1.5} \cdot 13H_2O$.

Assuming a continuous solid solution between Al- and Fe-ettringite the calculated ion concentrations agreed well with the measured concentrations, except for the ratio of $X_{Al,total} = 0.0$, where the measured concentrations were scattered (Fig. 6a). Although the standard deviation of the single measurements was small, the reproducibility seemed not to be that good. Fig. 6b shows the composition of the modeled solid phases. Since calcite was detected by TGA (see Fig. 3a and Table 2), $CO_2$ was additionally fed into the initial bulk composition of the modeled experiments corresponding to the observed amount of calcite in the solid phases.

Taking the results of XRD analysis into account, the ion concentration was modeled considering a miscibility gap between $X_{Al,total} = 0.25$ and 0.65. For modeling the binary Redlich–Kister model was used (Eq. (5)), which is based on Guggenheim's expansion series for the

**Table 3**
Measured ion concentrations in the aqueous solution.

| $X_{Al,total}$ | Measured pH | $OH^-$ [mmol/L] | Al [µmol/L] | Ca [mmol/L] | Fe [µmol/L] | S [mmol/L] | K [mmol/L] |
|---|---|---|---|---|---|---|---|
| 0.0 | 12.3 | 17 | 10.6 ± 0.1 | 14.90 ± 0.03 | 0.04 ± 0.04 | 24.42 ± 0.12 | 35.58 ± 0.11 |
| 0.0[a] | 12.2 | 17 | n.d. | 4.38 ± 0.01 | 0.094 ± 0.001 | 9.11 ± 0.07 | 26.45 ± 0.05 |
| 0.0[b] | 12.4 | 23 | n.d. | 3.95 ± 0.01 | 0.148 ± 0.001 | 5.54 ± 0.04 | 26.52 ± 0.05 |
| 0.1 | 12.3 | 13 | 7.5 ± 0.0 | 4.35 ± 0.00 | 0.5 ± 0.04 | 14.11 ± 0.18 | 33.04 ± 0.46 |
| 0.2 | 12.3 | 13 | 10.7 ± 0.1 | 3.53 ± 0.01 | 0.24 ± 0.05 | 13.26 ± 0.07 | 32.94 ± 0.13 |
| 0.3 | 12.3 | 17 | 12.0 ± 0.2 | 2.81 ± 0.01 | 0.18 ± 0.02 | 11.97 ± 0.08 | 33.89 ± 0.14 |
| 0.4 | 12.3 | 19 | 10.2 ± 0.4 | 3.15 ± 0.01 | 0.28 ± 0.14 | 11.50 ± 0.09 | 34.22 ± 0.07 |
| 0.5 | 12.3 | 20 | 10.4 ± 0.3 | 3.90 ± 0.05 | 0.57 ± 0.01 | 10.53 ± 0.04 | 33.63 ± 0.03 |
| 0.6 | 12.3 | 21 | 12.6 ± 0.3 | 3.06 ± 0.01 | 0.79 ± 0.07 | 9.79 ± 0.05 | 34.53 ± 0.07 |
| 0.7 | 12.2 | 20 | 10.3 ± 0.3 | 2.32 ± 0.01 | 0.41 ± 0.02 | 8.47 ± 0.02 | 32.61 ± 0.07 |
| 0.8 | 12.1 | 20 | 17.6 ± 0.6 | 1.72 ± 0.01 | 0.61 ± 0.07 | 7.36 ± 0.07 | 31.92 ± 0.06 |
| 0.9 | 12.1 | 19 | 1300 ± 17 | 0.27 ± 0.00 | 1.25 ± 0.06 | 5.48 ± 0.08 | 32.51 ± 0.39 |
| 1.0 | 12.2 | 20 | 1945 ± 40 | 0.25 ± 0.00 | 0.52 ± 0.01 | 4.30 ± 0.03 | 31.84 ± 0.03 |
| KOH-solution | | | 12.6 ± 0.4 | <DL | <DL | <DL | 33.34 ± 0.14 |
| Detection limit | – | – | <0.2 | <0.2 | <0.04 | <2.0 | <0.3 |

[a]Results from precipitation and [b]from dissolution experiments given in [29].
n.d.: not determined.
Detection limits are given for the undiluted solutions.

**Table 4**
Thermodynamic data given at 25 °C.

| Aqueous species | Reactions | log $K$ or log $\beta$ | Reference |
|---|---|---|---|
| | $Ca^{2+} + H_2O \leftrightarrows CaOH^+ + H^+$ | −12.78 | [33] |
| | $Ca^{2+} + SO_4^{2-} \leftrightarrows CaSO_4^0$ | 2.30 | [33] |
| | $Ca^{2+} + HCO_3^- \leftrightarrows CaHCO_3^+$ | 1.106 | [33] |
| | $Ca^{2+} + HCO_3^- \leftrightarrows CaCO_3^0 + H^+$ | −7.105 | [33] |
| | $K^+ + H_2O \leftrightarrows KOH^0 + H^+$ | −14.46 | [33] |
| | $K^+ + SO_4^{2-} \leftrightarrows KSO_4^-$ | 0.85 | [33] |
| | $H_2O \leftrightarrows OH^- + H^+$ | −14.00 | [33] |
| | $Fe^{3+} + H_2O \leftrightarrows Fe(OH)^{2+} + H^+$ | −2.19 | [33] |
| | $2Fe^{3+} + 2H_2O \leftrightarrows Fe_2(OH)_2^{4+} + 2H^+$ | −2.95 | [33] |
| | $3Fe^{3+} + 4H_2O \leftrightarrows Fe_3(OH)_4^{5+} + 4H^+$ | −6.30 | [33] |
| | $Fe^{3+} + 2H_2O \leftrightarrows Fe(OH)_2^+ + 2H^+$ | −5.67 | [33] |
| | $Fe^{3+} + 3H_2O \leftrightarrows Fe(OH)_3^0 + 3H^+$ | −12.56 | [33] |
| | $Fe^{3+} + 4H_2O \leftrightarrows Fe(OH)_4^- + 4H^+$ | −21.60 | [33] |
| | $Fe^{3+} + H^+ + SO_4^{2-} \leftrightarrows FeHSO_4^{2+}$ | 4.47 | [33] |
| | $Fe^{3+} + SO_4^{2-} \leftrightarrows FeSO_4^+$ | 4.04 | [33] |
| | $Fe^{3+} + 2SO_4^{2-} \leftrightarrows Fe(SO_4)_2^-$ | 5.38 | [33] |
| | $Al^{3+} + H_2O \leftrightarrows Al(OH)^{2+} + H^+$ | −4.96 | [33] |
| | $Al^{3+} + 2H_2O \leftrightarrows Al(OH)_2^+ + 2H^+$ | −10.59 | [33] |
| | $Al^{3+} + 3H_2O \leftrightarrows Al(OH)_3^0 + 3H^+$ | −16.43 | [33] |
| | $Al^{3+} + 4H_2O \leftrightarrows Al(OH)_4^- + 4H^+$ | −22.88 | [33] |
| | $Al^{3+} + SO_4^{2-} \leftrightarrows AlSO_4^+$ | 3.90 | [33] |
| | $Al^{3+} + 2SO_4^{2-} \leftrightarrows Al(SO_4)_2^-$ | 5.90 | [33] |
| **Minerals** | | **log $K_{S0}$** | **Reference** |
| Gypsum | $CaSO_4 \cdot 2H_2O(s) \leftrightarrows Ca^{2+} + SO_4^{2-} + 2H_2O$ | −4.58 | [33] |
| Portlandite | $Ca(OH)_2(s) + 2H^+ \leftrightarrows Ca^{2+} + 2H_2O$ | 22.80 | [33] |
| Calcite | $CaCO_3(s) + H^+ \leftrightarrows CaHCO_3^+$ | 1.849 | [33] |
| Fe-ettringite | $Ca_6[Fe(OH)_6]_2(SO_4)_3 \cdot 26H_2O \leftrightarrows 6Ca^{2+} + 2Fe(OH)_4^- + 3SO_4^{2-} + 4OH^- + 26H_2O$ | −44.0 | [29] |
| Al-ettringite | $Ca_6[Al(OH)_6]_2(SO_4)_3 \cdot 26H_2O \leftrightarrows 6Ca^{2+} + 2Al(OH)_4^- + 3SO_4^{2-} + 4OH^- + 26H_2O$ | −44.9 | [41] |
| $Fe(OH)_3$ (am.) | $Fe(OH)_3(am) + 3H^+ \leftrightarrows Fe^{3+} + 3H_2O$ | 5.00 | [33] |
| $Fe(OH)_3$ (microcr.) | $Fe(OH)_3(mic) + 3H^+ \leftrightarrows Fe^{3+} + 3H_2O$ | 3.30 | a |

(a) this paper.

excess Gibbs energy ($G_{EX}$) of mixing for non-ideal binary solid solutions.

$$G_{EX} = RT \cdot X_{Al-ettringite} \cdot X_{Fe-ettringite}\left[a_0 + a_1\left(X_{Al-ettringite} - X_{Fe-ettringite}\right)\right] \quad (5)$$

where $X_{Al\text{-}ettringite}$ stands for the mole fraction of Al-ettringite in the mix and $X_{Fe\text{-}ettringite}$ for the mole fraction of Fe-ettringite in the mix; $a_0$ and $a_1$ are the Guggenheim parameters; for further details see [34,42,43]. The dimensionless Guggenheim parameters (see Table 7) were calculated using the computer program MBSSAS [42]; these parameters were then fed into the model established by GEMS.

The calculated ion concentrations and the composition of the solid phases of the solid solution series with a miscibility gap between $X_{Al,total} = 0.25$ and 0.65 are presented (together with the experimental data) in Fig. 7. The modeled concentrations did not differ much from the calculated data of a continuous solid solution,

**Table 5**
Thermodynamic data of Al-ettringite and Fe-ettringite at 25 °C.

| | Al-ettringite [41] | Fe-ettringite [29] |
|---|---|---|
| $\Delta_f G^0$ in kJ/mol | −15206 | −14282 |
| $\Delta_f H^0$ in kJ/mol | −17535 | −16600 |
| $S^0$ in J/(mol K) | 1900 | 1937 |
| $C^0_p$ in J/(mol K) | 2174 | 2200 |
| $a_0$ | 1939 | 1922.384 |
| $a_1$ | 0.789 | 0.855 |
| $a_2$ | | 2,020,870 |

**Table 6**
Thermodynamic data at 20 and 25 °C used to calculate the apparent Gibbs free energy of formation of Al-ettringite and Fe-ettringite.

| Species | $\Delta_a G°$ [kJ/mol] at 20 °C | $\Delta_f G°$ [kJ/mol] at 25 °C | Reference |
|---|---|---|---|
| $H_2O_{liquid}$ | −236.835 | −237.183 | [45][a] |
| $OH^-$ | −157.318 | −157.270 | [45] |
| $Ca^{2+}$ | −553.071 | −552.790 | [45] |
| $CO_3^{2-}$ | −528.220 | 527.982 | [45] |
| $Al(OH)_4^-$ | −1301.298 | −1301.845 | [45] |
| $Fe(OH)_4^-$ | −841.696 | −842.624 | [45] |
| $SO_4^{2-}$ | −744.353 | −744.459 | [45] |
| Al-ettringite | −15196.53 | −15205.94 | b,[41] |
| Fe-ettringite | −14272.73 | −14282.36 | [29] |

[a] In GEMS, the log $K$ data of the PSI Database [33], which are applicable at standard pressure and temperature only, are merged with a subset of the supcrt database, as is documented in detail in [45].
[b] This study.

but between $X_{Al,total} = 0.6$ and 0.9 for sulfur and hydroxide ions the concentrations were somewhat higher and for calcium even clearly higher concentrations were calculated (see Fig. 7a). The model without a miscibility gap fitted somewhat better to the experimental data of the aqueous phase (cf. Figs. 6a and 7a), which was contrary to XRD results.

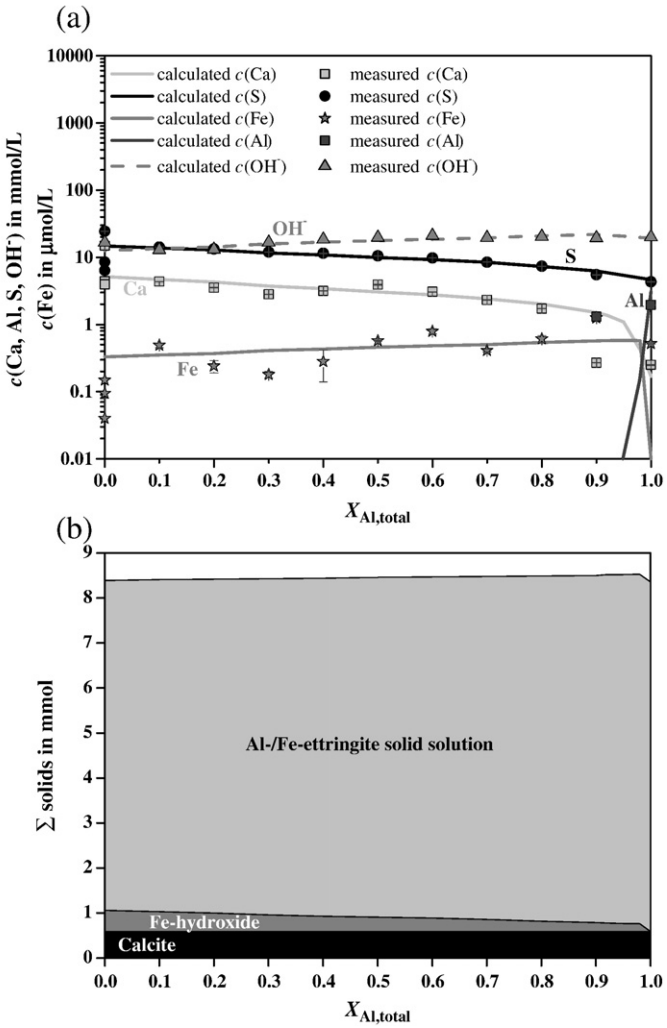


**Fig. 6.** (a) Measured and calculated concentrations of calcium (Ca), sulfur (S), iron (Fe), aluminum (Al), and $OH^-$ concentration in the aqueous solution for ettringite synthesized with different $X_{Al,total}$ ratios assuming a continuous solid solution and the formation of calcite and Fe-hydroxide. (b) Calculated solids assuming a continuous solid solution and the formation of calcite and Fe-hydroxide.

**Table 7**
Guggenheim parameters for a non-ideal solid solution between Al- and Fe-ettringite with a miscibility gap.

| Miscibility gap | 0.20–0.60 | 0.20–0.70 | **0.25–0.65** | 0.30–0.60 | 0.30–0.70 |
|---|---|---|---|---|---|
| Guggenheim parameter $a_0$ | 2.02 | 2.18 | **2.10** | 2.04 | 2.12 |
| Guggenheim parameter $a_1$ | −0.368 | −0.194 | **−0.169** | −0.153 | 0 |

The parameters used in the model are in bold.

Since the results obtained from experiments and modeling were ambiguous the solubility products of Fe-ettringite and Al-ettringite as well as the total solubility products of the solid solution series were determined. The dissolution reaction of $Ca_6[Al_{1-x}Fe_x(OH)_6]_2(SO_4)_3 \cdot 26H_2O$ is given by

$$Ca_6[Al(OH)_6 + Fe(OH)_6]_2(SO_4)_3 \cdot 26H_2O \leftrightarrows 6Ca^{2+} + 2((Al(OH)_4^- + Fe(OH)_4^-)) + 3SO_4^{2-} + 4OH^- + 26H_2O. \quad (6)$$

According to this dissolution reaction the total solubility product ($\Sigma\Pi$) can be calculated (cf. [42,44]).

$$\Sigma\Pi = \{Ca^{2+}\}^6 \cdot \{(Al(OH)_4^- + Fe(OH)_4^-)\}^2 \cdot \{SO_4^{2-}\}^3 \cdot \{OH^-\}^4 \cdot \{H_2O\}^{26} \quad (7)$$

where {} denotes the activity.

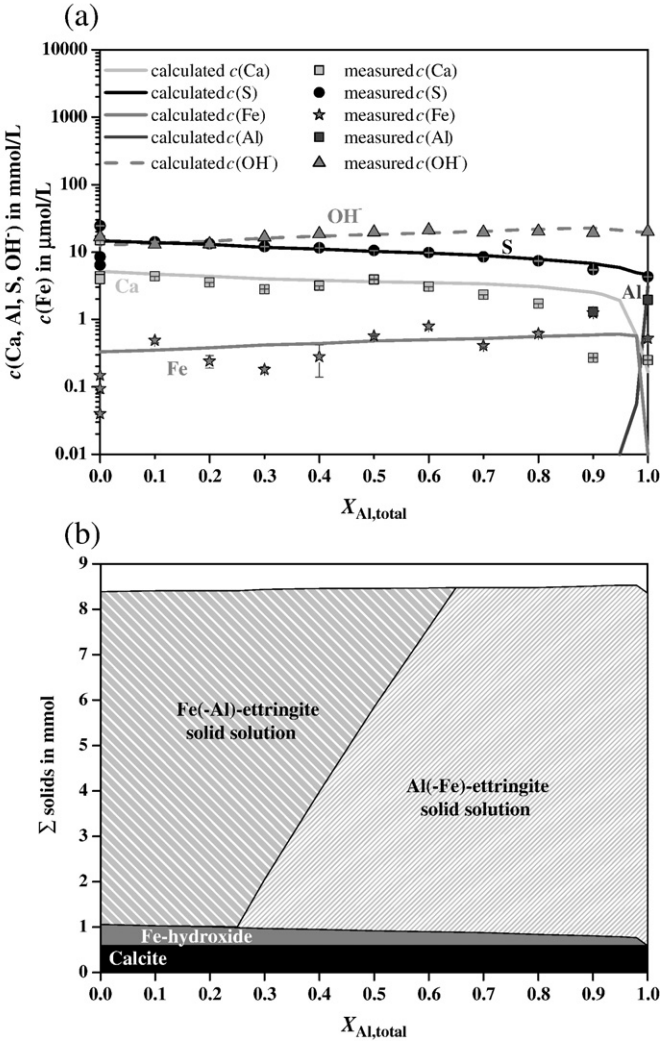


**Fig. 7.** (a) Measured and calculated concentrations of calcium (Ca), sulfur (S), iron (Fe), aluminum (Al), and $OH^-$ concentration in the aqueous solution for ettringite synthesized with different $X_{Al,total}$ ratios assuming a miscibility gap between $X_{Al,total}$ = 0.25–0.65 and the formation of calcite and Fe-hydroxide. (b) Calculated solids assuming a miscibility gap between $X_{Al,total}$ = 0.25–0.65 and the formation of calcite and Fe-hydroxide.

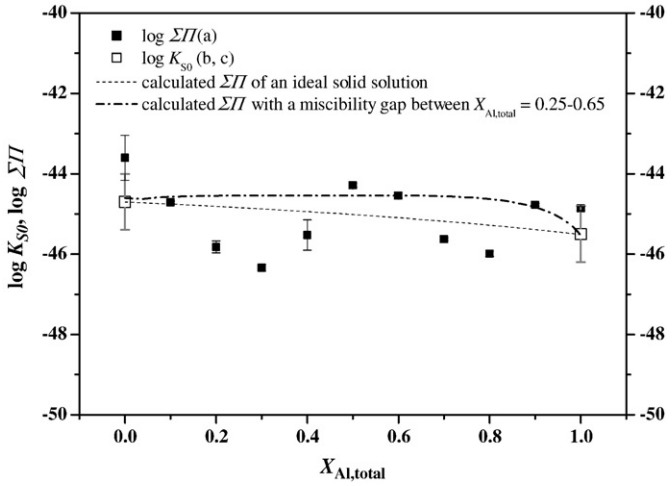


**Fig. 8.** Calculated and published solubility products of ettringite phases at different $X_{Al,total}$ ratios. (a) this study, (b) [29], and (c) [41].

On the basis of the measured ion concentrations and the analyzed composition of the solid phases, $\Sigma\Pi$ could be calculated with GEMS using the activities of the species for every sample. The calculated total solubility products at 20 °C are presented in Fig. 8. The obtained solubility products varied between log $\Sigma\Pi = -46.4$ ($X_{Al,total} = 0.3$) and log $\Sigma\Pi = -43.6$ ($X_{Al,total} = 0.0$) and did not show a clear trend. If the formation of an ideal solid solution was assumed, the modeled total solubility product between the two end members showed an almost linear trend, while, assuming a miscibility gap between $X_{Al,total} = 0.25$ and 0.65, $\Sigma\Pi$ stayed constant in the range of the miscibility gap, and then decreased abruptly from $X_{Al,total} = 0.85$–1.0. In the case of a miscibility gap the total solubility products are higher than for an ideal solid solution. Given the scatter of the experimentally determined solubilities it cannot be concluded if the observed solubilities represent an ideal solid solution or a miscibility gap. The measurements of the dissolved concentration of a single solubility experiment showed a good reproducibility and thus a low standard deviation (see Table 3 and Figs. 6–8). The reproducibility of such a solubility experiment, however, is much smaller as illustrated in Figs. 6–8. Small differences in the concentration of the different ion species result in relatively large difference in the total solubility product of the solid solution series of ettringite (cf. Eq. (7)). As the solubility products of pure Al- and Fe-ettringite differ only in 0.8 log units and as the standard deviation of the two end members is ±0.7 log units, the observed scatter of the total solubility products represented rather the scatter of the experimental data than any real trend. Hence, neither an ideal solid solution, nor a miscibility gap could be excluded by calculating the total solubility products.

## 5. Conclusion

Both, pure aluminum and pure iron ettringite are well investigated minerals. But the miscibility of these two phases has been sparingly investigated. Buhlert and Kuzel [11] suggested the presence of a miscibility gap between the molar ratios of $X_{Al,total} = 0.2$ to 0.3, since they found by XRD analysis a broadening of the main peak in this range. In this study XRD analysis indicated the presence of a miscibility gap between the molar ratios of $X_{Al,total} = 0.3$ and 0.6 in the solid solution series of Al- and Fe-ettringite. Four reflections (104, 114, 116 and 216) clearly showed two overlapping peaks for the samples from $X_{Al,total} = 0.3$ to $X_{Al,total} = 0.6$. Contrary to Buhlert and Kuzel [11], the *c*-axis showed not a gently but a sudden decline when more aluminum entered the solid phase. It should be noted that the synthesis method for the ettringite phases used by [11] (presence of excessive gypsum, no pH adjustment, slightly higher temperature, and

less equilibration time) was different than the method used in this study. Thus, any discrepancies can be most likely ascribed to these different synthesis methods.

Thermodynamic modeling was carried out to confirm the assumption of a miscibility gap in the solid solution series of Al- and Fe-ettringite. The calculated ion concentrations within the aqueous phase did not show a significant difference between the composition of the aqueous phases in equilibrium with a continuous solid solution or in equilibrium with a solid solution with a miscibility gap. In addition, the total solubility products (for both, ideal solid solution and miscibility gap) were modeled and compared with the experimentally obtained solubility data. Given the scatter of the experimentally determined solubilities it cannot be concluded if the observed solubilities represent an ideal solid solution or a miscibility gap.

Although the analyses of the aqueous phases were somewhat ambiguous, analyses of the solid phases indicated the existence of a miscibility gap for the solid solution series $Ca_6[Al_{1-x}Fe_x(OH)_6]_2(SO_4)_3 \cdot 26H_2O$ between $X_{Al,total} = 0.3$ and 0.6.

Finally, it has to be pointed out that within other systems, with different conditions to those used in these experiments, the formation of a solid solution series between Al- and Fe-ettringite can be preferred or inhibited. For example, the formation of Fe-ettringite is much slower than the formation of Al-ettringite [29], therefore for the formation of Al-/Fe-ettringite phases enough time is required. Higher temperature will lead to a diminution of the miscibility gap (see Eq. (5)).

## Acknowledgements

The authors would like to thank Luigi Brunetti for his support during laboratory work.

The financial support (Grant 20021-103546/1) of the Swiss National Foundation is gratefully acknowledged.

## References

[1] F.A. Bannister, Ettringite from Scawt Hill, Co. Antrim. Mineral. Mag. 6 (1936) 324–329.
[2] C.S. Hurlbut, J.L. Baum, Ettringite from Franklin, New Jersey, Am. Mineral. 45 (11/12) (1960) 1137–1143.
[3] P.J. Dunn, D.R. Peacor, P.B. Leavens, J.L. Baum, Charlesite, a new mineral of the ettringite group, from Franklin, New Jersey, Am. Mineral. 68 (1983) 1033–1037.
[4] D.R. Peacor, P.J. Dunn, M. Duggan, Sturmanite, a ferric iron, boron analogue of ettringite, Can. Mineral. 21 (1983) 705–709.
[5] K.A. Rodgers, S.F. Courtney, New mineral records from Funafuti, Tuvalu: gypsum, brucite, ettringite, Mineral. Mag. 52 (1988) 411–414.
[6] D. McConnell, J. Murdoch, Crystal chemistry of ettringite, Mineral. Mag. 15 (1962) 59–64.
[7] L.G. Berry, The unit cell of ettringite, Am. Mineral. 48 (July–August 1963) 939–940.
[8] A. Moore, H.F.W. Taylor, Crystal structure of ettringite, Nature 218 (5146) (1968) 1048.
[9] S.M. Antao, M.J. Duane, I. Hassan, DTA, TG and XRD studies of sturmanite and ettringite, Can. Mineral. 40 (2002) 1403–1409.
[10] D.Y. Pushcharovsky, Y.S. Lebedeva, N.V. Zubkova, M. Pasero, M. Bellezza, S. Merlino, N.V. Chukanov, The crystal structure of sturmanite, Can. Mineral. 42 (2004) 723–729.
[11] R. Buhlert, H.-J. Kuzel, Ueber den Einbau von $Cr^{3+}$ und $Fe^{3+}$ in Ettringit, ZKG Int. 2 (1971) 83–85.
[12] L.A. Galimova, V.P. Danilov, I.N. Lepeshkov, B.E. Yudovich, N.A. Shebanov, A study of the formation and decomposition of the calcium iron(III) double hydroxide sulphate $Ca_6Fe_2(OH)_{12}(SO_4)_3 \cdot 26H_2O$ in the $3Ca(OH)_2 + Fe_2(SO_4)_3 \rightarrow 3CaSO_4 + 2Fe(OH)_3$–$H_2O$ system at 20 °C, Russ. J. Inorg. Chem. 33 (3) (1988) 445–448.
[13] V. Albino, R. Cioffi, M. Marroccoli, L. Santoro, Potential application of ettringite generating systems for hazardous waste stabilization, J. Hazard. Mater. 51 (1996) 241–252.
[14] K. Wieczorek-Ciurowa, K. Fela, A.J. Kozak, Chromium(III)-ettringite formation and its thermal stability, J. Therm. Anal. Calorim. 65 (2001) 655–660.
[15] R.B. Perkins, C.D. Palmer, Solubility of $Ca_6[Al(OH)_6]_2(CrO_4)_3 \cdot 26H_2O$, the chromate analog of ettringite; 5–75 °C, Appl. Geochem. 15 (2000) 1203–1218.
[16] I. Baur, C.A. Johnson, The solubility of selenate-AFt ($3CaO \cdot Al_2O_3 \cdot 3CaSeO_4 \cdot 37.5H_2O$) and selenate-AFm ($3CaO \cdot Al_2O_3 \cdot CaSeO_4 \cdot xH_2O$), Cem. Concr. Res. 33 (2003) 1741–1748.
[17] M. Chrysochoou, D. Dermatas, Evaluation of ettringite and hydrocalumite formation for heavy metal immobilization: literature review and experimental study, J. Hazard. Mater. 136 (2006) 20–33.
[18] H.F.W. Taylor, Cement Chemistry, Thomas Telford Publishing, London, 1997.
[19] M. Collepardi, S. Monosi, G. Moriconi, Tetracalcium aluminoferrite hydration in the presence of lime and gypsum, Cem. Concr. Res. 9 (1979) 431–437.
[20] M. Fukuhara, S. Goto, K. Asage, M. Daimon, R. Kondo, Mechanisms and kinetics of $C_4AF$ hydration with gypsum, Cem. Concr. Res. 11 (3) (1981) 407–414.
[21] P.W. Brown, Kinetics of tricalcium aluminate and tetracalcium aluminoferrite hydration in the presence of calcium sulfate, J. Am. Ceram. Soc. 76 (12) (1993) 2971–2976.
[22] T. Liang, Y. Nanru, Hydration products of calcium aluminoferrite in the presence of gypsum, Cem. Concr. Res. 24 (1) (1994) 150–158.
[23] A. Emanuelson, S. Hansen, Distribution of iron among ferrite hydrates, Cem. Concr. Res. 27 (8) (1997) 1167–1177.
[24] J. Csizmadia, G. Balazs, F.D. Tamas, Chloride ion binding capacity of aluminoferrites, Cem. Concr. Res. 31 (2001) 577–588.
[25] N. Meller, C. Hall, A.C. Jupe, S.L. Colston, S.D.M. Jacques, P. Barnes, J. Phipps, The paste hydration of brownmillerite with and without gypsum: a time resolved synchrotron diffraction study at 30, 70, 100 and 150 °C, J. Mater. Chem. 14 (3) (2004) 428–435.
[26] L. Black, C. Breen, J. Yarwood, J. Phipps, G. Maitland, In situ Raman analysis of hydrating $C_3A$ and $C_4AF$ pastes in presence and absence of sulphate, Adv. Appl. Ceram. 105 (4) (2006) 209–216.
[27] H.-E. Schwiete, U. Ludwig, Crystal structures and properties of cement hydration products (hydrated calcium aluminates and ferrites), Proceedings of the Fifth International Symposium on the Chemistry of Cement, Tokyo, 1968.
[28] H.F. McMurdie, M.C. Morris, E.H. Evans, B. Paretzkin, W. Wong-Ng, Y. Zhang, Standard X-ray diffraction powder patterns from the JCPDS research associateship, Powder Diffr. 2 (1) (1987) 41–52.
[29] G. Möschner, B. Lothenbach, J. Rose, A. Ulrich, R. Figi, R. Kretzschmar, Solubility of Fe-ettringite ($Ca_6[Fe(OH)_6]_2(SO_4)_3 \cdot 26H_2O$), Geochim. Cosmochim. Acta 72 (1) (2008) 1–18.
[30] J. Neubauer, F. Götz-Neunhoeffer, D. Schmitt, M. Degenkolb, U. Holland, In-situ Untersuchungen der frühen PZ-Hydratation, Ibausil - 16, Internationale Baustofftagung, Tagungsbericht, Weimar, Germany, 2006.
[31] R.B. Perkins, C.D. Palmer, Solubility of ettringite ($Ca_6[Al(OH)_6]_2(SO_4)_3 \cdot 26H_2O$) at 5–75 °C, Geochim. Cosmochim. Acta 63 (13/14) (1999) 1969–1980.
[32] D.A. Kulik, GEMS-PSI 2.12, PSI Villigen, Switzerland; available at http://les.web.psi.ch/Software/GEMS-PSI/index.html.
[33] W. Hummel, U. Berner, E. Curti, F.J. Pearson, T. Thoenen, Nagra/PSI Chemical Thermodyanmic Data Base 01/01, Universal Publishers/uPublish.com, Parkland, Florida, 2002.
[34] G.M. Anderson, D.A. Crerar, Thermodynamics in Geochemistry. The Equilibrium Model, Oxford University Press, New York, Oxford, 1993.
[35] D.A. Kulik, Minimising uncertainty induced by temperature extrapolations of thermodynamic data: a pragmatic view on the integration of thermodynamic databases into geochemical computer codes, The Use of Thermodynamic Databases in Performance Assessment, OECD, Paris, Barcelona, Spain, 2002.
[36] F.J. Pearson, U. Berner, Nagra thermochemical data base. I. Core data, Nagra — Technical Report 91-17, Nagra, Wettingen (Switzerland), 1991.
[37] A.F. Hollemann, E. Wiberg, Lehrbuch der anorganischen Chemie, de Gruyter, Berlin, 1985.
[38] F. Goetz-Neunhoeffer, J. Neubauer, Refined ettringite ($Ca_6Al_2(SO_4)_3(OH)_{12} \cdot 26H_2O$) structure for quantitative X-ray diffraction analysis, Powder Diffr. 21 (1) (2006) 4–11.
[39] F. Goetz-Neunhoeffer, J. Neubauer, P. Schwesig, Mineralogical characteristics of ettringites synthesized from solutions and suspensions, Cem. Concr. Res. 36 (2006) 65–70.
[40] A.E. Moore, H.F.W. Taylor, Crystal structure of ettringite, Acta Crystallogr., B. 26 (1970) 386–393.
[41] B. Lothenbach, T. Matschei, G. Möschner, F.P. Glasser, Thermodynamic modelling of the effect of temperature on the hydration and porosity of Portland cement, Cem. Concr. Res. 38 (1) (2008) 1–18.
[42] P.D. Glynn, MBSSAS: a code for the computation of Margules parameters and equilibrium relations in binary solid-solution aqueous-solution systems, Comput. Geosci. 17 (7) (1991) 907–966.
[43] P. Glynn, Solid-solution solubilities and thermodynamics: sulfates, carbonates and halides, sulfate minerals — crystallography, geochemistry and environmental significance, Rev. Mineral. Geochem. 40 (2000) 481–511.
[44] P.D. Glynn, E.J. Reardon, L.N. Plummer, E. Busenberg, Reaction paths and equilibrium end-points in solid-solution aqueous-solution systems, Geochim. Cosmochim. Acta 54 (1990) 267–282.
[45] T. Thoenen, D.A. Kulik, Nagra/PSI Chemical Thermodynamic Data Base 01/01 for the GEM-Selektor (V.2-PSI) Geochemical Modeling Code: release 28-02-03, Internal report TM-44-03-04, 2003, available at http://les.web.psi.ch/software/GEMS-PSI/thermodata/index.html.